Active sieving across driven nanopores for tunable selectivity

Sophie Marbach, and Lydéric Bocquet

Citation: The Journal of Chemical Physics **147**, 154701 (2017);
View online: https://doi.org/10.1063/1.4997993
View Table of Contents: http://aip.scitation.org/toc/jcp/147/15
Published by the American Institute of Physics

Active sieving across driven nanopores for tunable selectivity

Sophie Marbach and Lydéric Bocquet[a)]
Laboratoire de Physique Statistique, UMR CNRS 8550, Ecole Normale Supérieure, PSL Research University, 24 Rue Lhomond, 75005 Paris, France

(Received 28 July 2017; accepted 18 September 2017; published online 17 October 2017)

Molecular separation traditionally relies on sieving processes across passive nanoporous membranes. Here we explore theoretically the concept of non-equilibrium active sieving. We investigate a simple model for an active noisy nanopore, where gating—in terms of size or charge—is externally driven at a tunable frequency. Our analytical and numerical results unveil a rich sieving diagram in terms of the forced gating frequency. Unexpectedly, the separation ability is strongly increased as compared to its passive (zero frequency) counterpart. It also points to the possibility of tuning dynamically the osmotic pressure. Active separation outperforms passive sieving and represents a promising avenue for advanced filtration. *Published by AIP Publishing.* https://doi.org/10.1063/1.4997993

I. INTRODUCTION

Filtering specific molecules is a challenge faced for numerous vital needs: from biomedical applications like dialysis to the intensive production of clean water.[1–3] Most modern processes for filtration are based on passive sieving principles: a membrane with specific pore properties allows us to separate the permeating components from the retentate. The domain has been boosted over the last two decades by the possibilities offered by nanoscale materials, such as graphene or advanced membranes.[4–12] Selectivity requires small and properly decorated pores at the scale of the targeted molecules, and this inevitably impedes the flux and transport, making separation processes costly in terms of energy. These traditional sieving membranes are also passive, therefore unable to adapt to external changes, like varying salt or contaminant concentrations in the liquid to filtrate. Furthermore while nature is able to distinguish quasi-similar ions, e.g., like sodium and potassium,[13] no artificial counterpart has been designed up to now to reach such a fine selectivity.

In this context, we explore the possibility of *active sieving*, harnessing non-equilibrium dynamics to separate particles across nanopores. A Maxwell demon is the (utopian) prototypical system able to perform separation on the basis of transfer of information.[14] However designing active pores that can distinguish between nanometer-scale molecules presents the obvious challenge of measuring *in situ* the proper information, i.e., fabricating feedback nanocontrollers.[15–17] Now one may consider a simpler situation of an active nanopore that can change its transmission properties with time thanks to an external energy input. This corresponds accordingly to a non-equilibrium situation, baring some analogy with active matter, which allows us to bypass to some extent the equilibrium constraints for better separation.

Here we explore a simple situation, where an external mechanical or electrical action modifies the pore properties, thus creating some blind, "crazy," Maxwell demon. Typical geometries of driven nanopores under consideration are sketched in Fig. 1: a driven nano-gate, a pore with a fluctuating size, or a pore whose surface charge may be externally gated. Such geometries are of special interest in the present study since they are amenable to further experimental investigations. To model separation across these systems, we build on the pioneering work of Zwanzig in Refs. 18 and 19, who considered the translocation rate of molecules through fluctuating pores. We consider as a supplementary ingredient that the opening of the nanopore is forced externally at a given frequency ω.

II. AN ACTIVE PORE MODEL

A. Effusion of solute through an active pore

We consider the effusion of a solute (with concentration C in a reservoir) across a nanopore. Pore gating that controls the translocation state across the nanopore is characterized by an internal parameter x: for example, the radius of the pore, the door opening, or the surface charge, see Fig. 1. In line with Zwanzig's model in Refs. 18 and 19, we assume that the solute concentration C relaxes according to the following leakage equation:

$$\frac{dC}{dt} = -K(x)C, \tag{1}$$

where $K(x)$ is the x-dependent leakage constant. It is proportional to the mobility of the solute. It also depends on the characteristics of the gating. For steric gating, x is merely geometrical: for the circular pore in Fig. 1(b), x is the radius r of the pore and $K(r) = k' r^2$, while for the nanodoor, x is the aperture of the door and $K(x) = k|x|$. For electric gating, when the pore is charged, see Fig. 1(c), x is proportional to the surface charge of the pore Σ, and for small nanopores, one may model $K(x) = k''\sqrt{1+x^2}$ (see Appendix A for details). The constant k (respectively, k' and k'') defines the mobility of the solute.

a)Electronic mail: lyderic.bocquet@lps.ens.fr

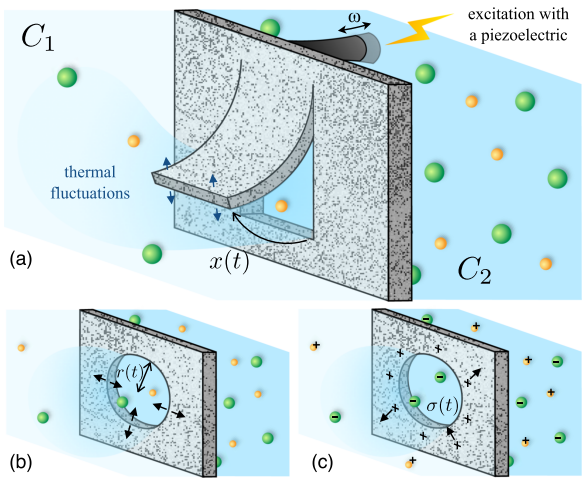

FIG. 1. (a) A driven nanodoor in a membrane, submitted to opening by thermal fluctuations and by external application of a periodic excitation. (b) Circular nanopore with fluctuating size and (c) with fluctuating charge.

We are interested in the separation of small sized particles (say, ions, colloids, polymers, etc.) effusing through nanometric sized pores. Accordingly the internal parameter x is further assumed to evolve dynamically due to (i) thermal noise, expected at the nanoscale, and (ii) some external forcing that drives an oscillation. To simplify the discussion, we assume that the nanopore is excited such that its *average* opening x oscillates at a frequency ω, and we further model the effects of thermal noise by a simple Langevin equation for the excess internal parameter $\delta x = x - \langle x \rangle$,

$$\begin{aligned} \langle x \rangle &= x_0(t) = x_0 \sin(\omega t), \\ \frac{d\,\delta x}{dt} &= -\lambda \delta x + F(t), \end{aligned} \tag{2}$$

where $F(t)$ is the Gaussian white noise. The second moment of δx is $\langle \delta x^2 \rangle = \theta$, and the fluctuation-dissipation theorem at equilibrium imposes $\langle F(t)F(t') \rangle = 2\theta\lambda\delta(t-t')$. The goal now is to obtain more information on the evolution of the solute concentration averaged over the noise: $\langle C(t) \rangle$.

B. From a rate process to the Smoluchowski equation

We turn to the equivalent Fokker-Planck—or Smoluchowski—equation for C. This derivation is inspired by Ref. 18. We denote $f(C,x,t)$ as the probability distribution that the variables C and x have specified values at time t. This function satisfies the Liouville equation

$$\frac{\partial f}{\partial t} = -\frac{\partial}{\partial C}\left(\frac{dC}{dt} f\right) - \frac{\partial \frac{dx}{dt} f}{\partial x} \tag{3}$$

or, substituting the velocities explicitly,

$$\begin{aligned} \frac{\partial f}{\partial t} &= -\frac{\partial}{\partial C}\left(-K(x) C f\right) \\ &\quad - \frac{\partial\left(-\lambda(x - x_0) f + \frac{dx_0}{dt} f + F(t) f\right)}{\partial x}. \end{aligned} \tag{4}$$

Now we would like to average this stochastic Liouville equation to have the average of f over the noise: $g(C,r,t) = \langle f(C,r,t) \rangle_{\text{noise}}$. We may rewrite the Liouville equation in terms of an operator L such that Eq. (4) is

$$\frac{\partial f}{\partial t} = -Lf - \frac{\partial F(t) f}{\partial x}. \tag{5}$$

It integrates into

$$f(C,r,t) = e^{-tL} f(C,x,0) - \int_0^t ds e^{-(t-s)L} \frac{\partial F(s) f}{\partial x}, \tag{6}$$

which we use to rewrite the differential equation as

$$\frac{\partial f}{\partial t} = -Lf - \frac{\partial F(t)\left(e^{-tL} f(C,r,0) - \int_0^t ds e^{-(t-s)L} \frac{\partial F(s) f}{\partial x}\right)}{\partial x}. \tag{7}$$

Now we can safely average over the noise, using the Gaussian properties of $F(t)$, namely, $\langle F(t) \rangle = 0$ and $\langle F(t)F(t') \rangle = 2\theta\lambda\delta(t-t')$, which gives

$$\frac{\partial g}{\partial t} = -Lg + \frac{\partial \lambda\theta \frac{\partial g}{\partial x}}{\partial x}. \tag{8}$$

Now we look for the average value of C at time t and key feature x: $\bar{C}(x,t) = \int dC C g(C,x,t)$. This yields the following differential equation (Smoluchowski equation):

$$\frac{\partial \bar{C}}{\partial t} = -K(x)\bar{C} + \frac{\partial}{\partial x}\lambda\theta\frac{\partial \bar{C}}{\partial x} + \frac{\partial\left(\lambda(x - x_0) - \frac{dx_0}{dt}\right)\bar{C}}{\partial x}. \tag{9}$$

C. Permeance of the active pore

The time-dependent concentration $\langle C(t) \rangle$ is accordingly defined as $\int \bar{C}(x,t)dx = \langle C(t) \rangle$. For simplicity in the following, we consider that the noise damping parameter λ does not depend on x. The Smoluchowski equation, Eq. (9), can be solved analytically for some specific forms of $K(x)$ [in particular, for $K(x) \propto x^2$]. Alternatively we solve Eq. (9) numerically to deduce the time-dependent averaged concentration $\langle C(t) \rangle$. We show in Fig. 2 an example for the averaged concentration $\langle C(t) \rangle$, here in the case of a nanodoor where $K(x) = k|x|$ [Fig. 1(a)].

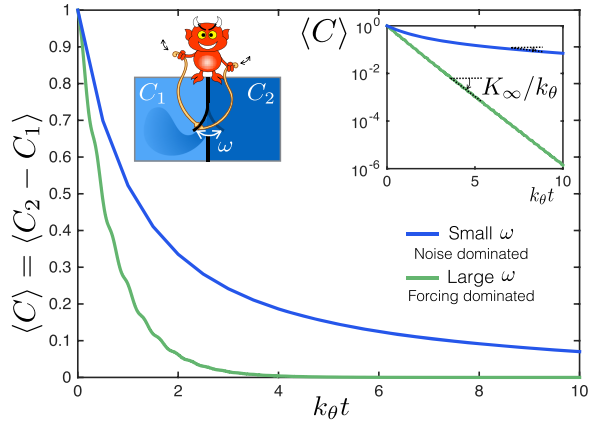

FIG. 2. Relaxation of the difference in concentration between the two sides of a nanodoor, averaged over noise. The data are a simulation result with $\lambda/k_\theta = 10^{-3}$, $\omega/k_\theta = 10^{-3}$, and $\omega/k_\theta = 1$. (*Inset*, *Left*) Illustration of a demon oscillating the nanodoor. (*Inset*, *Right*) Log scale of the previous graph and example of the extraction of the long time relaxation constant K_∞, the *permeance* of the system.

As a generic feature, one may show that $\langle C(t)\rangle$ is exponentially decaying at long times,

$$\langle C(t)\rangle \underset{t\to\infty}{\sim} \exp(-K_\infty t), \tag{10}$$

and this allows us to define the *permeance* K_∞ of the system. Fast translocation of the solute corresponds to a large K_∞. The permeance K_∞ depends on the thermal damping λ, noise amplitude θ, but also on the external forcing (frequency ω and amplitude x_0). In the following, our goal is to identify general rules on how the permeance depends on these antagonistic effects. Units of lengths are given by $\sqrt{\theta}$, while time is given in terms of a renormalized parameter k_θ with units of an inverse time: for the nanodoor, $k_\theta = k\sqrt{\theta}$, while for the nanopore, $k_\theta = k'\theta$.

III. TRANSPORT THROUGH THE ACTIVE PORE

Let us first focus on an oscillating circular pore, in which case the leakage law writes as $K(r) = k'r^2$, with r as the pore radius, see Fig. 1(b). We study fluctuations around the averaged forced radius $\langle r(t)\rangle = r_0(1+\epsilon\cos(\omega t))$ with a given amplitude $r_0\epsilon$. In this case, the Smoluchowski equation can be solved analytically (see Appendix B), and the expression for the permeance is written as

$$K_\infty(\omega) = \lambda/2\left(\left(1+\frac{4k'\theta}{\lambda}\right)^{1/2}-1\right)+k'r_0^2\left(1+\frac{4k'\theta}{\lambda}\right)^{-1} + k'\frac{r_0^2\epsilon^2}{2}\left(\frac{\left(1+\frac{4k'\theta}{\lambda}\right)^{-1}}{1+\left(\frac{\omega}{\omega_c(\lambda)}\right)^2}+\frac{\left(\frac{\omega}{\omega_c(\lambda)}\right)^2}{1+\left(\frac{\omega}{\omega_c(\lambda)}\right)^2}\right) \tag{11}$$

with $\omega_c(\lambda) = \sqrt{4k'\theta\lambda+\lambda^2}$ as the cutoff frequency. The first term in Eq. (11) corresponds to the solution for the non-forced case studied by Zwanzig in Ref. 19. In Zwanzig's derivation, only fluctuations of a bottleneck opening are considered (with a hard reflecting barrier at $r = 0$ so that only positive radii are considered). With $r_0 = 0$ and $\omega = 0$, one recovers exactly the exponential factor of Eq. (8) of Ref. 19. The last term corresponds to the supplementary leakage induced by the forced oscillations: it is the combination of a low-pass filter and a high-pass filter. The general behavior of $K_\infty(\omega)$ is plotted in Fig. 3(a). It exhibits complex features that are summarized in the diagram of Fig. 3(b). Although it is presented here only for the nanopore, the diagram is generic to all the systems investigated and represented in Fig. 1.

Let us discuss the various regimes at play. It is first interesting to explore the limiting behaviors at low damping. This regime is actually relevant for ionic or liquid separation systems;[4,20] see, for instance, the experimental study of biological channels in Ref. 21 which is consistent with the low damping limit relaxation with $\lambda \propto 1/\eta$, with η as the fluid viscosity. For low and high frequencies, we can calculate from Eq. (11) (at highest order)

$$\begin{aligned} K_\infty(\omega) &\underset{\substack{\omega\ll\omega_c\\ \lambda\ll k_\theta}}{\sim} \sqrt{k'\lambda\theta}, \\ K_\infty(\omega) &\underset{\substack{\omega\gg\omega_c\\ \lambda\ll k_\theta}}{\sim} k'r_0^2\epsilon^2/2. \end{aligned} \tag{12}$$

These results call for a generic physical interpretation. At high frequency, the forced oscillations become too quick for the thermal damping to rub them out and K_∞ reduces simply to its noise average: $K_\infty \simeq (\omega/2\pi)\int K[x_0(t)]dt$. This is the *forcing dominated regime*; see Fig. 3(d). The behavior at low forcing frequencies ω, where noise dominates [see Fig. 3(c)], is more subtle. According to Eq. (2), the gating variable will mainly diffuse with a diffusion coefficient $\mathcal{D}_x = \theta\lambda$. Over a time τ, the gating variable thus takes a typical value $\bar{x} \sim \sqrt{\mathcal{D}_x\tau}$. Now the passage time is itself fixed by K_∞^{-1} so that one gets a self-consistent estimate for K_∞ as

$$K_\infty \underset{\substack{\omega\ll\omega_c\\ \lambda\ll k_\theta}}{\simeq} K\left[\bar{x}\sim\sqrt{\frac{\lambda\theta}{K_\infty}}\right]. \tag{13}$$

For the circular nanopore, where x is the radius r and $K(r) = k'r^2$, one deduces accordingly $K_\infty \approx \sqrt{k'\lambda\theta}$ as obtained in

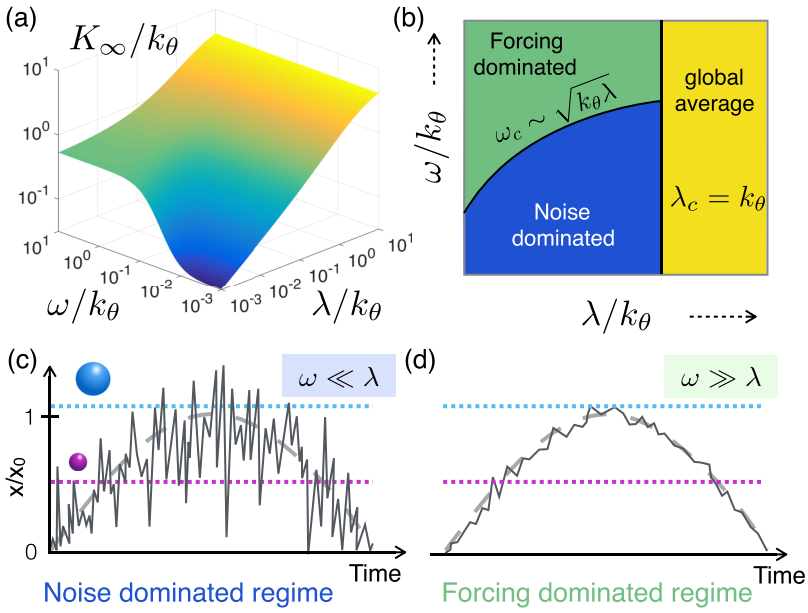

FIG. 3. (a) Analytical solution of the permeance K_∞ as a function of the forcing frequency ω and the thermal damping λ for the forced nanopore system ($r_0 = 2\sqrt{\theta}$ and $\epsilon = 0.5$). (b) Universal phase diagram of the permeance K_∞ with ω and λ. (c) Schematic of the door opening x/x_0 (solid black line) in the noise dominated regime, where $\omega \ll \lambda$, and (d) in the forcing dominated regime, where $\omega \gg \lambda$.

Eq. (12). This interpretation for K_∞ in Eq. (13) can be generalized to the other types of gates. For the nanodoor, for which $K(x) = k|x|$, Eq. (13) predicts $K_\infty \approx (k\lambda\theta)^{1/3}$, as can indeed be verified numerically (see Appendix C).

The transition between the low and high frequency regimes results from the competition between the forced oscillations and the noise. In Eq. (2) the thermal fluctuations $f(t)$ compete with the forced oscillations $dx_0(t)/dt \sim \omega x_0(t)$, and the crossover between the two regimes occurs accordingly when $f(t) \sim dx_0(t)/dt$. Using the fluctuation-dissipation theorem and taking a typical time scale $\tau \sim k_\theta^{-1}$, this yields $\omega_c(\lambda) \sim \sqrt{k_\theta \lambda}$ for the critical frequency. This estimation perfectly matches the scaling obtained numerically for all systems in Fig. 1 and also with the full analytical expression, Eq. (11), for the circular pore in Fig. 1(b).

IV. DYNAMICAL SELECTIVITY

A. Dynamical gating on mobility

The different scalings in Eq. (12) suggest further that the passage rate K_∞ exhibits a strongly contrasted dependence on the particle mobility (via k') in the low and high frequency regimes. Accordingly, at finite frequency, solutes with different mobilities will be separated by the active gate in a very different way as compared to the static (passive) nanopore.

This is highlighted in Figs. 4(a)–4(c), where we show the permeance of the nanopore to particles of different permeabilities, corresponding to particles with different k' (here $k_1/k_2 = 100$ for illustration). The selectivity of the pore, defined in terms of the ratio of the permeances of the two particles, is plotted in Fig. 4(c). What is striking in this plot is that the selectivity is a strongly dependent function of the frequency (and furthermore non-monotonous) so that the relative translocation rate of the two species can be finely tuned by the forcing frequency. This stems from the fact that the critical frequency ω_c for each particle is dependent on the particle mobility (via k'). Thus, a slower-diffusing particle will reach the forcing dominated regime at smaller frequencies. When the slower (blue) particle has just transitioned to the forcing dominated regime, the faster (purple) particle is still in the noise dominated regime, and the selectivity is reduced. This points to various non-trivial avenues for "on demand" sieving.

We emphasize that these results are not dependent on the choice of relative mobility, and here $k_1/k_2 = 100$ is chosen for readability. In a more realistic case of ionic separation, for instance, separating sodium and potassium, we would have $k^{(K^+)}/k^{(Na^+)} = 1.47$.[22] As a consequence, for low frequencies, the selectivity $K_\infty^{(K^+)}/K_\infty^{(Na^+)} \sim \sqrt{k^{(K^+)}/k^{(Na^+)}} \sim 1.21$, and at high frequencies, the selectivity increases: $K_\infty^{(K^+)}/K_\infty^{(Na^+)} \sim k^{(K^+)}/k^{(Na^+)} \sim 1.47$. Note that this does not depend on the value of the noise damping parameter λ: as long as noise is significant in the system, one will always find the critical frequencies from one regime to another.

B. Dynamical gating on size

This behavior is generic to all gatings described in Fig. 1. To highlight this generic feature, we conclude by considering the dynamical selectivity of the nanodoor, represented in Fig. 1(a), with a slightly modified gating process taking explicitly in consideration the effect of the finite size of the particle, see Fig. 4(d). We use a similar gating function as in Ref. 23 so that particles cannot pass if the opening x of the pore is smaller than their size x_p. We modify accordingly the leakage law of Eq. (1) to $K(x - x_p)\mathcal{H}(x - x_p)$, where $\mathcal{H}$ is the Heaviside function. For this leakage law, the Smoluchowski equation cannot be solved analytically and we turn to numerical solutions, see Appendix C. In Fig. 4(e) we compare the measured permeance for three particle sizes: an infinitely small particle (size 0 in grey), a small particle (in purple), and a large particle (in blue). As above, we deduce the corresponding selectivity factor for the two particles with different sizes as the ratio of their permeance. As obtained above for the other gating processes, we find a selectivity that is dependent on the frequency, here a strongly increasing function of the frequency.

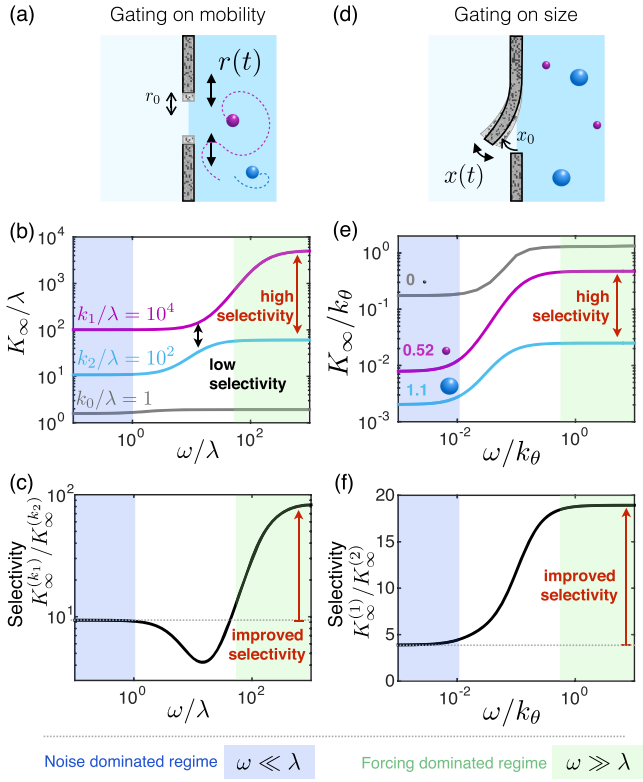

FIG. 4. (a) Schematic of gating through the fluctuating pore relying on mobility differences between particles. (b) Permeance K_∞/λ through the nanopore of two particles with mobility $k_1/\lambda = 10^4$ and $k_2/\lambda = 10^2$ as a function of the forcing frequency ω/λ, for small λ. (c) Selectivity of the nanopore to those particles, defined as the ratio of the permeances. (d) Schematic of gating through the fluctuating door relying on size differences between particles. (e) Permeance K_∞/k_θ through the nanodoor of two particles of different sizes (the smallest, purple, is $0.52x_0$ in radius and the largest, blue, is $1.1x_0$) as a function of the forcing frequency ω/k_θ, for small λ. (f) Selectivity of the nanodoor to those particles, defined as the ratio of their permeances.

V. DISCUSSIONS AND CONCLUSIONS

A. General conclusion

These results show that the selectivity of nanoporous membranes can finely be tuned by an externally forced

gating. Depending on the forcing frequency, dynamical gating allows us to better discriminate particles with different sizes or mobilities. As a rule, in the limit of low damping common in liquid or ionic filtration, an active pore is thus capable of filtering more precisely smaller particles than a standard passive filter with fixed pore size (at zero frequency). Also, in the high frequency regime, an active pore sieves particles in terms of their mobility, which is interesting to separate particles with similar size or charge (as would be needed for the separation of ions, for instance, for distinguishing sodium and potassium that have similar size and charge but different mobilities).[22] Although simple, our model provides a rich diagram, highlighting noise dominated or forcing dominated regimes, with specific selectivity rules. These selectivity properties may be tuned by adjusting the frequency of the excitation and rely on the strong interplay between noise and external excitation.

Numerous extensions can be obviously proposed for the model, which we now plan to explore exhaustively. The model could be easily exploited to explore the consequences of several extensions. If the noise damping parameter λ now depends on x, one expects the critical frequency ω_c and the limiting regimes to be modified in a non-trivial way. Furthermore, since the equations are not linear, when a non-monochromatic excitation is triggered, mode coupling will occur and may result into a broader variety of behaviors. Another underlying question in the prospect of possible applications of this research—in particular within the field of desalination and filtration—is that of the energy consumption of such a device. Obviously the active or dynamical part of the sieving requires some energy input; however, that energy input depends on the specific means of excitation and a detailed energy balance is required to predict the energy efficiency of such dynamical sieving process, a question which we leave for future work.

However the present results already suggest a number of developments for experimental implementations of active pores. Nanoporous materials with piezoelectric or piezomechanical response, e.g., metal organic frameworks,[24,25] are promising candidates in this goal. Furthermore, a nanodoor like in Fig. 1(a) can be designed by nanofabrication techniques, e.g., carving membranes at the sub-micron scale using a focused ion beam. Forcing at a tunable frequency, as well as supplementary white noise, can be provided by piezoelectric systems, allowing us to explore the various domains in the dynamical sieving diagram. These possibilities are a few examples for experimental realizations. They constitute natural routes for a proof of concept of the ideas presented here.

B. Towards an on-demand osmotic pressure

We conclude with a final comment on osmotic pressure. As highlighted by Kedem and Katchalsky in the context of membrane transport, there is an intimate symmetry link between permeance and osmosis.[26] A non-vanishing (respectively, vanishing) osmotic pressure is expressed for a semi-permeable (respectively, fully permeable) membrane. This link is highlighted by the generic expression for the osmotic pressure[26]

$$\Delta\Pi = \sigma \times k_B T \langle C \rangle \tag{14}$$

introducing the rejection coefficient σ, whose value is equal to 1 (respectively, 0) for a semi-permeable (respectively, fully permeable) membrane; for a finite permeance K_∞ of the membrane, one then expects $1 - \sigma \propto K_\infty$.[26] Going to dynamical sieving, the pore opening occurs intermittently with the frequency ω supplemented by thermal noise so that an intermittent osmotic pressure builds up. Let us explicit this link using the extended model with steric gating, with leakage law $K(x - x_p)\mathcal{H}(x - x_p)$ leading to an effective permeance $K_\infty(\omega|x_p)$. The corresponding solute flux $J_s = K_\infty \mathcal{V}\langle C \rangle$ (where $\mathcal{V}$ is the volume of the reservoir) can be identified to its definition $J_s = \overline{\mathcal{A}}\frac{D}{e}\kappa\langle C \rangle$, where $\overline{\mathcal{A}}$ is the average opening area of the pore, D is the diffusion coefficient of the solute, and e is the thickness of the membrane; the permeability coefficient κ is accordingly related to σ as $\kappa \propto 1 - \sigma$.[26] Gathering definitions, one thus obtains the dynamical rejection coefficient in terms of selectivity,

$$\sigma(\omega) = 1 - \frac{K_\infty(\omega|x_p)}{K_\infty(\omega|x_p = 0)}, \tag{15}$$

where the permeance of a particle with vanishing size $x_p = 0$ is used as normalization. This leads to a frequency dependent osmotic pressure, $\Delta\Pi(\omega) = \sigma(\omega) \times k_B T\langle C \rangle$. Note that this expression for the osmotic pressure is pertinent on time scales longer than the time-dependent forcing.

Our previous results for $K_\infty(\omega|x_p)$ show that $\Delta\Pi(\omega)$ is a strongly dependent function of ω via active sieving. This frequency dependence of the osmotic pressure is illustrated in Fig. 5 for various solutes. Tuning the frequency of the forcing therefore allows us to modify "on demand" the osmotic pressure across the active membrane. This opens new avenues in terms of separation for active and "on-demand" reverse osmosis.

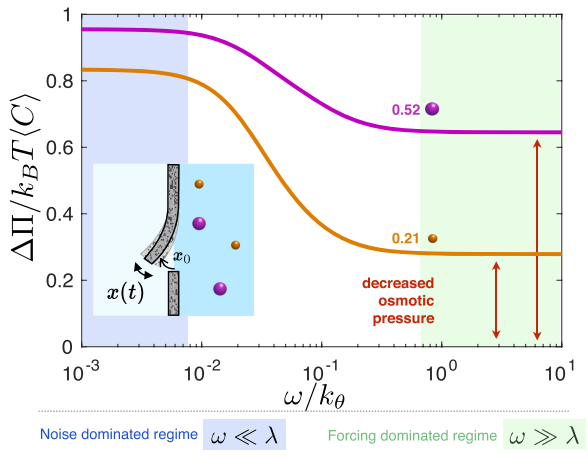

FIG. 5. Frequency dependent osmotic pressure through the nanodoor for two particles of different sizes (the largest, purple, is $0.52x_0$ in radius and the smallest, orange, is $0.21x_0$) as a function of the forcing frequency ω/k_θ for small λ. Inset: schematic of gating through the fluctuating door relying on size differences between particles.

ACKNOWLEDGMENTS

The authors thank R. Netz, A. Siria, and V. Kaiser for valuable discussions. S.M. acknowledges funding from a J.-P. Aguilar grant of the CFM foundation.

APPENDIX A: EXAMPLES OF RATE PROCESS LAWS

1. Strictly diffusion limited processes through pores

The initially concentrated reservoir has volume $\mathcal{V}$. The concentration at the scale of the pore is equilibrating over the typical thickness e of the pore with $\mathcal{A}$ as the pore's apparent section. We can write

$$\frac{dC}{dt} = -\frac{D}{\mathcal{V}e}\mathcal{A}C.$$

In the case of the nanodoor, $\mathcal{A} \sim x(h+w)$, where x is the opening depth of the door (see Fig. 1), h is the height of the door, and w is its width. As a consequence, we find

$$\frac{dC}{dt} = -k|x|C, \text{ with } \mathrm{k} = \frac{\mathrm{D(h+w)}}{\mathcal{V}\mathrm{e}} \tag{A1}$$

for the case of the nanodoor. We find that k is directly proportional to the mobility—or the diffusion coefficient—of the solute.

In the case of the circular pore $\mathcal{A} = \pi r^2$, where r is the radius of the circular pore. As a consequence, we find

$$\frac{dC}{dt} = -k'r^2C, \text{ with } k' = \frac{D\pi}{\mathcal{V}\mathrm{e}} \tag{A2}$$

for the case of the circular pore. This is the expression used in Ref. 19.

2. Charge influenced rate process

Transport in a narrow charged channel of apparent section $\mathcal{A}$ can be described within the one-dimensional Nernst-Planck model from Ref. 27. For the linear response, the relation between generalized fluxes and potentials is expressed via a transport coefficient matrix,

$$\begin{pmatrix} I \\ \Phi_t \end{pmatrix} = \frac{\mathcal{A}}{e}\begin{pmatrix} K & \mu_K \\ \mu_K & \mu_{\mathrm{eff}} \end{pmatrix} \cdot \begin{pmatrix} -\Delta V \\ -kT\Delta(\log C_s) \end{pmatrix},$$

$$K = 2\mu q^2\sqrt{C_s^2 + \left(\frac{\Sigma}{h}\right)^2},$$

$$\mu_{\mathrm{eff}} = 2\mu\sqrt{C_s^2 + \left(\frac{\Sigma}{h}\right)^2},$$

$$\mu_K = 2\mu q\frac{\Sigma}{h},$$

where Σ is the number of surface charge, h is the channel height, $\mu = \beta D$ is the ionic mobility, and q is the elementary charge.

We assume small initial concentration difference ΔC_s (around the value C_s) between two reservoirs of volume $\mathcal{V}$; therefore, we approximate $\Delta(\log C_s) \simeq (\Delta C_s)/C_s$. We apply no voltage difference; therefore, we focus on the equation

$$\frac{\mathrm{d}\Delta C_s}{\mathrm{d}t} = \frac{2\Phi_t}{\mathcal{V}} = -\frac{2\mathcal{A}}{e\mathcal{V}}\mu_{\mathrm{eff}}kT\Delta(\log C_s) \simeq -\frac{4D\mathcal{A}}{e\mathcal{V}}\sqrt{1+\left(\frac{\Sigma}{hC_s}\right)^2}\Delta C_s$$

and finally

$$\frac{\mathrm{d}C}{\mathrm{d}t} = -k''\sqrt{1+\sigma^2}C, \tag{A3}$$

where we relabeled the variables ($\Delta C_s \to C$, $\Sigma/hC_s \to \sigma$) in the last equation and introduced the characteristic rate $k'' = 4D\mathcal{A}/e\mathcal{V}$. Note that σ is the Dukhin number for the channel.

APPENDIX B: EXACT SOLUTION OF THE RATE PROCESS FOR CIRCULAR NANOPORES

We consider the case where an external force excites the radius of the pore at the frequency ω around a non-zero mean value so that

$$\langle r(t)\rangle_{noise} = r_0(1+\varepsilon\sin(\omega t)). \tag{B1}$$

The Smoluchowski equation (9) becomes

$$\frac{\partial\bar{C}}{\partial t} = -kr^2\bar{C} + \lambda\theta\frac{\partial^2\bar{C}}{\partial r^2} + \frac{\partial}{\partial r}\left(\left[\lambda(r - r_0(1+\varepsilon\sin(\omega t))) - r_0\varepsilon\omega\cos(\omega t)\right]\bar{C}\right). \tag{B2}$$

We assume that the probability distribution $\bar{C}$ initially has its equilibrium value in the absence of leakage, which simply writes as $\bar{C}(r, t=0) = \exp(-\frac{1}{2\theta}(r-r_0)^2)$.

We look for a solution writing as $\bar{C}(r,t) = \exp(a(t) + b(t)r - c(t)r^2)$. This yields the following system of equations:

$$\dot{a}(t) = -2\lambda\theta c + b^2\lambda\theta + \lambda - br_0(\varepsilon\omega\cos\omega t + \lambda(1+\varepsilon\sin\omega t)), \tag{B3a}$$

$$\dot{b}(t) = \lambda b - 4bc\theta\lambda + 2cr_0(\varepsilon\omega\cos\omega t + \lambda(1+\varepsilon\sin\omega t)), \tag{B3b}$$

$$\dot{c}(t) = k - 4c^2\lambda\theta + 2\lambda c. \tag{B3c}$$

We begin with Eq. (B3c) which has the general solution

$$c(t) = \frac{1}{4\theta}\left(1 + S\tanh\left(\lambda S(t-t_0)\right)\right),$$

where t_0 is a constant that can be computed thanks to initial conditions and $S = \left(1+\frac{4k\theta}{\lambda}\right)^{1/2}$. The initial conditions prescribe

$$c(t=0) = \frac{1}{2\theta} = \frac{1}{4\theta}\left(1 + S\tanh\left(-\lambda St_0\right)\right)$$

so that $\mathrm{th}\,(-\lambda St_0) = 1/S$. Replacing this result in the expression for c gives

$$c(t) = \frac{1}{4\theta}\left(\frac{2 + (S + 1/S)\tanh\lambda St}{1 + 1/S\tanh\lambda St}\right). \tag{B4}$$

The differential Eq. (B3b) is solved using the simple trick to write $b(t) = b_0(t)b_1(t)$, where $b_0(t)$ verifies the time

differential equation involving the terms depending on b only,

$$\dot{b}_0(t) = -\lambda b_0 \left(\frac{1 + S \tanh \lambda St}{1 + 1/S \tanh \lambda St} \right), \tag{B5}$$

and so $b_0(t) = 1/(S \cosh \lambda St + \sinh \lambda St)$. The equation on b_1 is then

$$\dot{b}_1(t) = 2c(t) r_0 (\varepsilon\omega \cos \omega t + \lambda(1 + \varepsilon \sin \omega t))/b_0(t) \tag{B6}$$

and we find the integration constant such that $b(t = 0) = r_0/\theta$. A lengthy but straightforward calculation leads to the solution of this equation as

$$\begin{aligned} b(t) = & \frac{r_0}{2S\,(S^2\lambda^2 + \omega^2)\,(S \cosh[St\lambda] + \sinh[St\lambda])} \cdots \\ & \times \Big((-1 + S^2)(\omega^2 + S^2\lambda(\lambda - \varepsilon\omega)) + \cosh[St\lambda] \cdots \\ & \times ((1 + S^2)(S^2\lambda^2 + \omega^2) + S^2(S^2 - 1)\varepsilon\lambda\omega \cos[\omega t] \\ & + S^2\epsilon((1 + S^2)\lambda^2 + 2\omega^2) \sin[\omega t]) \\ & + S(2(S^2\lambda^2 + \omega^2) + (-1 + S^2)\epsilon\lambda\omega \cos[\omega t] \\ & + \epsilon(\omega^2 + S^2(2\lambda^2 + \omega^2)) \sin[\omega t]) \sinh[St\lambda] \Big). \end{aligned} \tag{B7}$$

Using similar lines, one can also calculate the solution for $a(t)$ with the boundary condition $a(t = 0) = -r_0^2/(2\theta)$. The solution is not reported here because it is very lengthy.

We can now derive the average value on noise,

$$\left\langle \bar{C}(t) \right\rangle = \sqrt{\frac{\pi}{c(t)}} \exp\left(a(t) + \frac{b^2(t)}{4c(t)} \right). \tag{B8}$$

We then find that $\left\langle \bar{C}(t) \right\rangle$ behaves as

$$\left\langle \bar{C}(t) \right\rangle = \exp(-K_\infty(\omega)t + k_0(t)), \tag{B9}$$

where $k_0(t)$ is a small and periodic time contribution, which is sublinear in time and thus negligible for long time scales. $K_\infty(\omega)$ is the permeance and is such that

$$\left\langle \bar{C}(t) \right\rangle \underset{t\to\infty}{\sim} \exp(-K_\infty(\omega)t), \tag{B10}$$

with

$$K_\infty(\omega) = \lambda/2(S - 1) + k r_0^2 \left(\frac{1}{S^2} + \frac{\epsilon^2}{2} \frac{\lambda^2 + \omega^2}{S^2\lambda^2 + \omega^2} \right). \tag{B11}$$

By replacing $S = (1 + \frac{4k'\theta}{\lambda})^{1/2}$, we find exactly the result of Eq. (11).

APPENDIX C: NUMERICAL METHODS AND SOLUTIONS

1. Numerical methods

The Smoluchowski equations are solved with a finite difference scheme over 4 orders of magnitude of both ω and λ. Several methods are used to ensure global convergence.

- *Change in space variable.* We define $\tilde{C}(x, t) = \bar{C}(x - x_0(t), t)$ such that $\tilde{C}$ obeys a simpler Smoluchowski equation (no variation of the drift coefficient in time) and solve for $\tilde{C}$ instead of $\bar{C}$.
- *Logarithmic scale.* We define and solve for $\hat{C} = \log \tilde{C}$. This yields a non-linear equation, but the advantage is that high precision is gained—the initial condition is indeed a Gaussian and behaves much better (on a smaller number of orders of magnitude) in the Gaussian scale.
- *Partial Cranck-Nicholson.* We perform the Cranck Nicholson scheme on the linear part and explicit propagation on the non-linear part. Auto-adaptive time scale is used to check for convergence in time.
- The initial time step is chosen via a burning algorithm that allows us to adapt for any kind of parameters in the (ω, λ) parameter space.
- It was found that around a discretization of 1000 space steps usually gave reasonably convergent results. This number had to be adapted for different values in the parameter space anyway to ensure optimal convergence.
- K_∞ was computed as an average over several periods (usually 10) of the relaxation rate, after an initial reasonably long transient phase. A very small amount of configurations (less than 10 over 100 points), with high λ and small ω, would relax to numerically untractable small concentrations before a single oscillation period expired. Averaging over several periods was thus impossible. The data obtained for these very few very small frequencies were equated with the values obtained for higher frequencies at the same λ, for plotting purposes. At these high λ, K_∞ is not expected to depend on ω.

2. Systematic analysis in the absence of forcing

Limiting behaviors in the case of very high damping $\lambda \gg 1$, x has almost the equilibrium distribution at all times, and thus the transition ability can be approximated by

$$K_\infty \underset{\lambda\gg 1}{=} \int K(x)\rho_{eq}(x)dx. \tag{C1}$$

In the case of very low damping, we expect the following scaling discussed in the main paper:

$$K_\infty \underset{\lambda\ll 1}{=} K(\sqrt{\lambda/K_\infty}). \tag{C2}$$

Note that when the leakage law is a power law of the type $K(x) = |x|^n$, with n some integer, then one easily finds

$$K_\infty \sim \lambda^{\frac{n}{2+n}}. \tag{C3}$$

Equivalently, since the mobility λ depends inversely on the viscosity η of the fluid, $K_\infty \sim \eta^{-\frac{n}{2+n}}$.

In the following, we check these scaling laws for different rate processes. The results are summarized within the following paragraphs.

Quadratic rate process: Correspondence between simulations of the quadratic rate process and its exact solution was verified as a benchmark. We do not report this checking procedure here because it adds nothing to the discussion.

Linear rate process: In the following paragraph, we consider the leakage law associated typically with the nanodoor

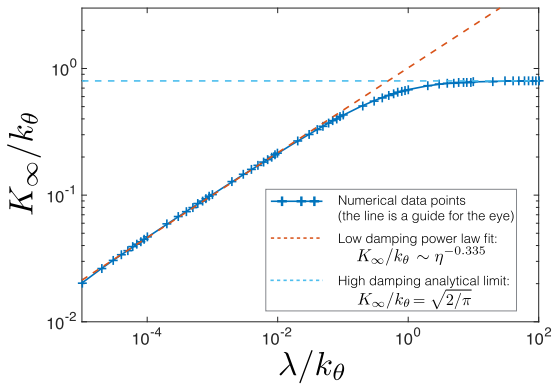

FIG. 6. Linear rate process permeance in the absence of forcing (nanodoor). Simulation results for the permeance K_∞ as a function of the thermal damping λ and comparison to analytical estimates. In this analysis, $k_\theta = k\sqrt{\theta}$. η is the viscosity of the fluid and is proportional to $1/\lambda$.

in Fig. 1(a), $K(x) = k|x|$. In Fig. 6 we show the permeance of the linear rate process as computed numerically. It verifies well the predicted low damping scaling law $K_\infty \sim \lambda^{1/3}$. The high damping limit is computed thanks to Eq. (C1) and is also in very good agreement with numerical calculations.

Note that in order to probe the previous scaling argument, $K_\infty \sim \lambda^{\frac{n}{2+n}}$, we also probed numerically other exponents in the leakage laws. For example, for a cubic leakage law ($n = 3$), the numerical resolution yields an exponent of 0.58, to compare with the analytic estimate of $3/(2+3) = 0.6$.

Charge regulated rate process: We finally consider the leakage law associated typically with the charged nanopore of Fig. 1(c), $K(\sigma) = k''\sqrt{1+\sigma^2}$. In Fig. 7 we show the permeance of the charge regulated process. The process has more features because in the present case θ accounts for the fluctuations of the (dimensionless) surface charge σ. In Fig. 7(a) we observe the permeance at different θ and find that for small λ and large θ, the system behaves as if it had an average leakage law behaving as $K(\sigma) \sim k'' + k''\sigma^2$, i.e., with an exponent $n = 2$. This correspondence is not obvious *a priori* but allows us to predict the scaling behavior for K_∞. Indeed, one may

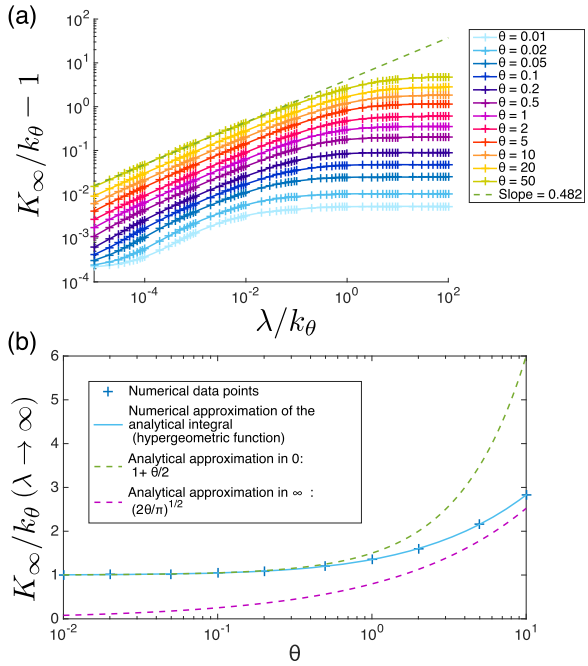

FIG. 7. Charge regulated rate process permeance in the absence of forcing. (a) Simulation results for the permeance K_∞ as a function of the thermal damping λ and comparison to analytical estimates. In this analysis, $k_\theta = k''$. θ is kept in the derivation and varied. The dashed green line verifies $K_\infty/k_\theta - 1 \propto (\lambda/k_\theta)^\beta$ with $\beta \simeq 0.482$. (b) Simulation results for the permeance K_∞ as a function of θ at high thermal damping λ and comparison to analytical estimates.

write that typically the diffusion time scales like $1/(K_\infty - 1)$, and one may then recover from Eq. (C1) that $K_\infty - 1 \sim \lambda^{1/2}$. This scaling prediction is confirmed numerically, see Fig. 7(a). In the regime of high damping, see Fig. 7(b), we find that the system is well described by the analytical expression Eq. (C1) for any θ.

3. Systematic analysis with forcing

We now perform simulations with an external forcing at frequency ω and check that we get for the different

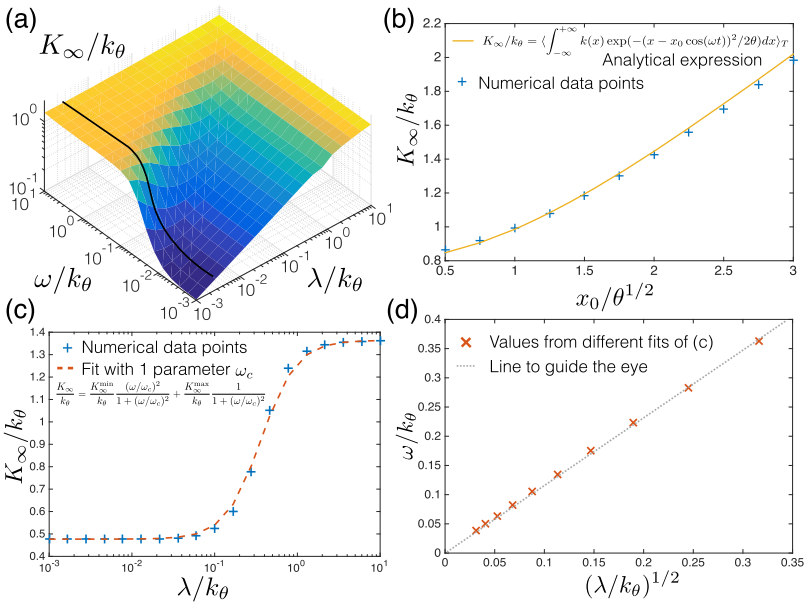

FIG. 8. Linear rate process permeance. (a) Simulation results for the permeance K_∞ as a function of the thermal damping λ and the forcing frequency ω and comparison to analytical estimates. In this analysis, $k_\theta = k\sqrt{\theta}$. The simulation parameter for oscillations around the origin is $x_0/\sqrt{\theta} = 2$. The black line indicates the fitting procedure at a given λ to find ω_c. (b) High plateau value for $\lambda/k_\theta = 10$ and $\omega/k_\theta = 0.1$ for different values of the ratio $x_0/\sqrt{\theta}$, where x_0 is the amplitude of the forcing $x_0(t) = x_0\cos\omega t$. (c) Example of a filter fit to determine ω_c from the permeance as a function of ω at a fixed $\lambda = 0.1k_\theta$. The type of filter used is given in the legend and the only fitting parameter is ω_c. (d) Plot of ω_c as determined according to (c) as a function of $\sqrt{\lambda}$.

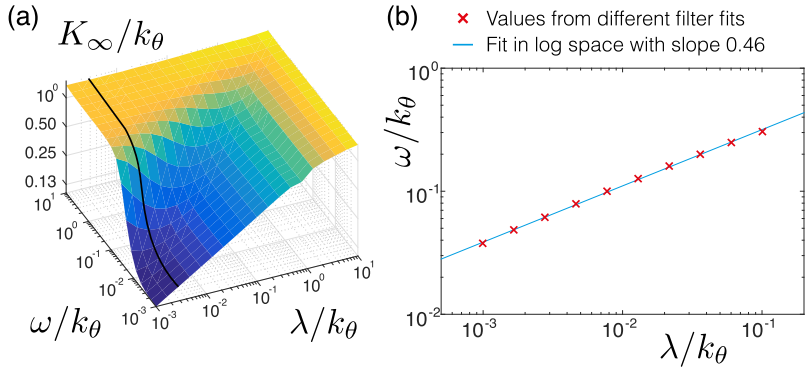

FIG. 9. Charge regulated rate process permeance. (a) Simulation results for the permeance K_∞ as a function of the thermal damping λ and the forcing frequency ω. In this analysis, $k_\theta = k''$. The simulation parameter for oscillations around the origin is $\sigma_0/\sqrt{\theta} = 2$, and $\theta = 1$. The black line indicates the fitting procedure at a given λ to find ω_c. (b) Plot of ω_c as determined from filter fits as a function of λ and power law fit.

systems (nanodoor and charged pore in Figs. 8 and 9) the same "universal features" as for the case of the circular pore. As for the circular nanopores, we indeed find 3 regimes: a forcing dominated regime, a noise dominated regime, and a global average regime, as described in the main text.

We also want to check some analytic scaling laws on the rate process theory with forcing at frequency ω. We have first considered the predicted scaling of the critical frequency with λ (see main text),

$$\omega_c(\lambda) \sim \sqrt{\lambda}. \tag{C4}$$

We performed a fit of each simulation (at constant λ) of K_∞ with the shape of a high pass filter (with a plateau at low frequencies) similar to the function H. We accordingly extract for each λ the value of ω_c and then find the scaling law between λ and ω_c. Overall we have verified that for all systems, the threshold frequency ω_c does obey this scaling law over a range of $\lambda \sim 10^{-3} \to 10^{-1}$.

Furthermore, we can check that the plateau value for the permeance at high λ matches the expected prediction assuming that x reaches its equilibrium distribution [see Fig. 8(b)]. Since the equilibrium distribution of x depends on t (it is periodic over a period $T = \frac{2\pi}{\omega}$), we should also average over a period. This writes as

$$K_\infty \underset{\lambda \gg 1}{=} \left\langle \int K(x)\rho_{eq}(x - x_0(t))dx \right\rangle_T. \tag{C5}$$

Quadratic rate process: As above, the correspondence between simulations of the quadratic rate process at various frequencies and its exact solution was verified before moving onto cases not solvable analytically. This test procedure is not shown here because it does not add to the discussion.

Linear rate process: In this paragraph, we consider the leakage law associated typically with the nanodoor of Fig. 1(a), $K(x) = k|x|$.

In Fig. 8(a) we show the permeance of the nanodoor system over 4 ranges of frequencies and damping. We find the three regimes of permeance (noise dominated regime in blue, forcing dominated regime in orange, and global average in yellow). The fitting procedure, described in Fig. 8(c), allows us to find ω_c for each λ. In Fig. 8(d) we plot ω_c as a function of $\sqrt{\lambda}$ and find a perfect agreement, which confirms the analytical prediction that $\omega_c \propto \sqrt{\lambda}$. The high plateau value [in yellow in Fig. 8(a)] for various forcing amplitudes is shown in Fig. 8(b) and agrees well with the prediction of Eq. (C5).

Charge regulated rate process: Finally we consider the leakage law associated typically with the charged nanopore in Fig. 1(c), $K(\sigma) = k''\sqrt{1+\sigma^2}$. In Fig. 9 we show the permeance of the charged pore over 4 orders of magnitude in frequency and damping. We find the three regimes of permeance (noise dominated regime in blue, forcing dominated regime in orange, and global average in yellow). The fitting procedure yields a typical dependence $\omega_c(\lambda) \sim \lambda^{0.46}$, see Fig. 9(b) very close to the analytical exponent (0.5).

[1]M. Elimelech and W. Phillip, "The future of seawater desalination: Energy, technology, and the environment," Science **333**, 712–717 (2011).
[2]L. Bocquet and P. Tabeling, "Physics and technological aspects of nanofluidics," Lab Chip **14**, 3143–3158 (2014).
[3]J. Werber, C. Osuji, and M. Elimelech, "Materials for next-generation desalination and water purification membranes," Nat. Rev. Mater. **1**, 16018 (2016).
[4]S. Y. Noskov, S. Berneche, and B. Roux, "Control of ion selectivity in potassium channels by electrostatic and dynamic properties of carbonyl ligands," Nature **431**, 830–834 (2004).
[5]T. Humplik, J. Lee, S. C. O'Hern, B. A. Fellman, M. A. Baig, S. F. Hassan, M. A. Atieh, F. Rahman, T. Laoui, R. Karnik, and E. N. Wang, "Nanostructured materials for water desalination," Nanotechnology **22**, 292001 (2011).
[6]J. Lee, T. Laoui, and R. Karnik, "Nanofluidic transport governed by the liquid/vapour interface," Nat. Nanotechnol. **9**, 317–323 (2014).
[7]J. K. Holt, H. G. Park, Y. Wang, M. Stadermann, A. B. Artyukhin, C. P. Grigoropoulos, A. Noy, and O. Bakajin, "Fast mass transport through sub-2-nanometer carbon nano-tubes," Science **312**, 1034 (2006).
[8]R. K. Joshi, P. Carbone, F. C. Wang, V. G. Kravets, Y. Su, I. V. Grigorieva, H. A. Wu, A. K. Geim, and R. R. Nair, "Precise and ultrafast molecular sieving through graphene oxide membranes," Science **343**, 752–754 (2014).
[9]A. Siria, P. Poncharal, A.-L. Biance, R. Fulcrand, X. Blase, S. T. Purcell, and L. Bocquet, "Giant osmotic energy conversion measured in a single transmembrane boron nitride nanotube," Nature **494**, 455–458 (2013).
[10]Z. Siwy and A. Fuliński, "Fabrication of a synthetic nanopore ion pump," Phys. Rev. Lett. **89**, 198103 (2002).
[11]C. B. Picallo, S. Gravelle, L. Joly, E. Charlaix, and L. Bocquet, "Nanofluidic osmotic diodes: Theory and molecular dynamics simulations," Phys. Rev. Lett. **111**, 244501 (2013).
[12]J. Feng, M. Graf, K. Liu, D. Ovchinnikov, D. Dumcenco, M. Heiranian, V. Nandigana, N. R. Aluru, A. Kis, and A. Radenovic, "Single-layer MoS_2 nanopores as nanopower generators," Nature **536**, 197 (2016).
[13]R. Greger and E. Schlatter, "Properties of the basolateral membrane of the cortical thick ascending limb of Henle's loop of rabbit kidney," Pfluegers Arch. Eur. J. Physiol. **396**, 325–334 (1983).
[14]L. Szilard, "Uber die entropieverminderung in einem thermodynamischen system bein eingriffen intelligenter wesen," Z. Phys. **53**, 840–856 (1929).
[15]B. Tavakol, M. Bozlar, C. Punckt, G. Froehlicher, H. A. Stone, I. A. Aksay, and D. P. Holmes, "Buckling of dielectric elastomeric plates for soft, electrically active microfluidic pumps," Soft Matter **10**, 4789–4794 (2014).

[16]J. Koski, V. Maisi, J. Pekola, and D. Averin, "Experimental realization of a Szilard engine with a single electron," Proc. Natl. Acad. Sci. U. S. A. **111**, 13786–13789 (2014).
[17]Y. Jun, M. Gavrilov, and J. Bechhoefer, "High-precision test of Landauer's principle in a feedback trap," Phys. Rev. Lett. **113**, 190601 (2014).
[18]R. Zwanzig, "Rate processes with dynamical disorder," Acc. Chem. Res. **23**, 148–152 (1990).
[19]R. Zwanzig, "Dynamical disorder: Passage through a fluctuating bottleneck," J. Chem. Phys. **97**, 3587–3589 (1992).
[20]E. Secchi, A. Niguès, L. Jubin, A. Siria, and L. Bocquet, "Scaling behavior for ionic transport and its fluctuations in individual carbon nanotubes," Phys. Rev. Lett. **116**, 154501 (2016).
[21]D. Beece, L. Eisenstein, H. Frauenfelder, D. Good, M. Marden, L. Reinisch, A. Reynolds, L. Sorensen, and K. Yue, "Solvent viscosity and protein dynamics," Biochemistry **19**, 5147–5157 (1980).
[22]D. R. Lide, *CRC Handbook of Chemistry and Physics, Volume 85* (CRC Press, 2004).
[23]N. Eizenberg and J. Klafter, "Molecular motion under stochastic gating," Chem. Phys. Lett. **243**, 9–14 (1995).
[24]D.-W. Fu, W. Zhang, and R.-G. Xiong, "The first metal–organic framework (MOF) of imazethapyr and its SHG, piezoelectric and ferroelectric properties," Dalton Trans. 3946–3948 (2008).
[25]A. U. Ortiz, A. Boutin, K. J. Gagnon, A. Clearfield, and F.-X. Coudert, "Remarkable pressure responses of metal–organic frameworks: Proton transfer and linker coiling in zinc alkyl gates," J. Am. Chem. Soc. **136**, 11540–11545 (2014).
[26]O. Kedem and A. Katchalsky, "Permeability of composite membranes. Part 1–3," Trans. Faraday Soc. **59**, 1918–1953 (1963).
[27]L. Bocquet and E. Charlaix, "Nanofluidics, from bulk to interfaces," Chem. Soc. Rev. **39**, 1073–1095 (2010).